THE JOURNAL OF PHYSICAL CHEMISTRY C

ARTICLE

pubs.acs.org/JPCC

Correlation and Morphology of Dopant Decomposition in Mn and Co Codoped Ge Epitaxial Films

James R. Riley,[†] Daniel E. Perea,[†,∥] Liang He,[‡] Frank Tsui,[‡] and Lincoln J. Lauhon*[,†]

[†]Department of Materials Science and Engineering, Northwestern University, 2220 Campus Drive, Evanston Illinois 60208, United States

[‡]Department of Physics and Astronomy, University of North Carolina, Chapel Hill, North Carolina 27599, United States

ABSTRACT: Atom probe tomography (APT) was used to quantify inhomogeneities in the distribution of Mn and Co in doped epitaxial Ge thin films for which X-ray diffraction (XRD) studies indicate single phase material. The segregation of dopants into Co and Mn-rich regions with characteristic sizes was evident upon visual inspection of the APT reconstruction and a frequency distribution analysis of the concentration of Co, Mn, and Ge atoms verified that the composition fluctuations exceeded those of a random alloy. Isoconcentration surfaces were generated to establish the connectedness of regions enriched in Mn that have been proposed to enhance the Curie temperature in dilute magnetic semiconductors. The analysis demonstrates important contributions that APT can make to the understanding of magnetism in these materials.

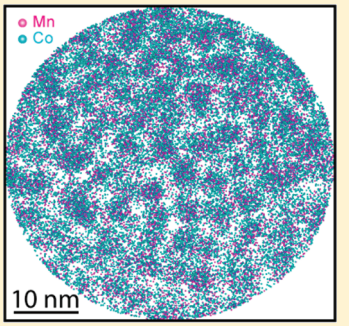

INTRODUCTION

Room-temperature ferromagnetic semiconductors that enable voltage-controlled spin alignment could lead to new device technologies including nonvolatile memory and logic devices with faster switching speeds and lower power consumption than charge-based devices.[1,2] Significant effort over the past decade has been directed toward the development of high Curie temperature dilute magnetic semiconductors (DMS) by doping group III−V and group-IV hosts with paramagnetic dopant atoms, especially Mn.[3,4] Ge is an appealing host because it has high intrinsic hole mobility and relatively high Curie temperature when doped with Mn.[3−7] As with III−V materials, however, the low solubility of Mn in Ge leads to solute segregation,[7] and the precipitation of secondary phases when the Mn content is on the order of a few percent.[3,4,8−11] The formation of regions enriched in the magnetic dopant, including dimers,[12] clusters,[3,7,9,11] and secondary phases,[4] complicates the interpretation of magnetization measurements because magnetic ordering in DMS materials depends sensitively on the local environment of the dopants and their spatial distribution. Unfortunately, conventional structural analysis techniques may not provide evidence of alloy decomposition even when magnetization and magnetotransport measurements provide evidence of inhomogeneous magnetic ordering.[2,7,13−15] X-ray diffraction, for example, does not detect segregation in the absence of secondary phase formation. In addition, XRD samples volumes over several micrometers and is rather insensitive to compositional variations involving elements of similar atomic number, especially if the variation is incoherent and aperiodic. Transmission electron microscopy (TEM) and scanning TEM (STEM) provide much higher (nonaveraged) spatial resolution than XRD methods, but it is very challenging to concurrently achieve high spatial resolution and general elemental sensitivity in STEM because a small probe size implies a small excitation volume.[13] The projection of 3-D information into 2-D is also rather limiting: even when qualitative evidence of few nm clusters may be evident,[3] one cannot quantitatively determine the distributions of the sizes and shapes of clusters, nor their connectedness, which would be extremely useful input to theory.

In contrast, atom probe tomography (APT) is an elemental mapping method that can determine the composition of solids with single atom sensitivity and subnanometer spatial resolution.[16] Knowledge of the distribution of individual atoms in three dimensions enables the construction of real-space distribution and correlation functions, such as radial distribution functions, that provide completely new insight into material structure at the nanometer scale. Uniform Mn doping of $Ga_{0.963}Mn_{0.037}As$ thin films has been reported by APT analysis,[17] but the technique has only recently been applied to analysis of group-IV DMS materials, where Mn dopant segregation was observed in $Ge_{1-x}Mn_x$.[11] Here we report APT analysis of the inhomogeneous distribution of Mn and Co in doped epitaxial Ge thin films for which XRD studies indicate single phase material.[18] Previously, the addition of a second dopant Co was shown to stabilize Mn against secondary phase precipitation for doping concentrations as high as 15 at. %.[6,18] The segregation of dopants into regions with higher Mn and Co content than the surrounding matrix is evident upon visual inspection of the APT reconstruction, and a frequency distribution analysis of the concentration of Co, Mn, and Ge atoms verifies that the fluctuations in

Received: September 5, 2011
Revised: November 26, 2011
Published: December 16, 2011

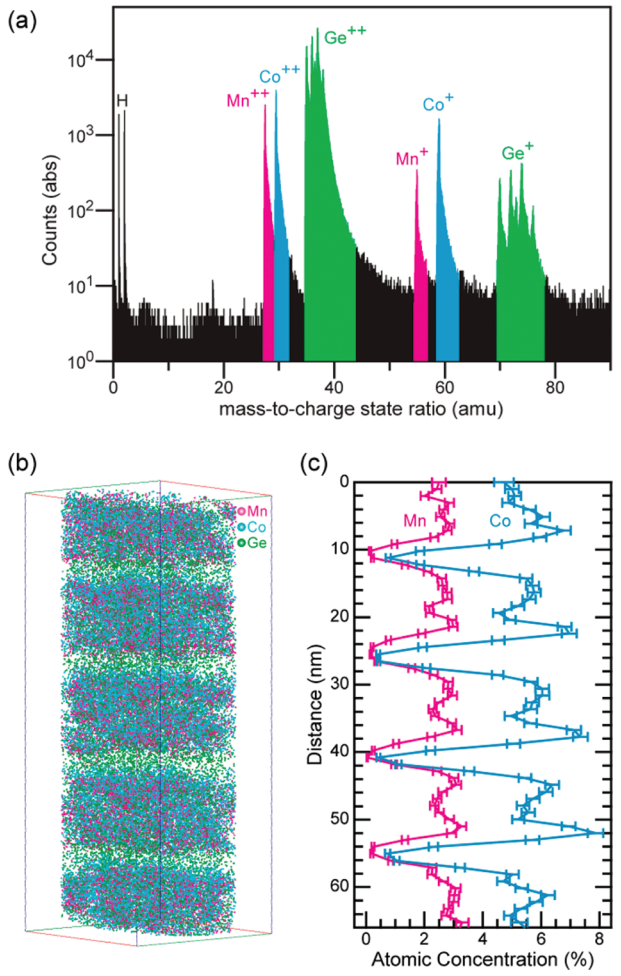

Figure 1. (a) Mass spectrum collected while performing APT. (b) 3-D reconstruction of the Ge/GeCoMn superlattice structure. 100% of Co and Mn atoms are displayed while only 2% of Ge atoms are shown for clarity. (dimensions: 26 × 26 × 66 nm^3). (c) 1-D concentration profile of Mn and Co atoms taken in the axial direction of the sample.

composition exceed those of a random alloy. Regions significantly enriched in dopants appear connected throughout the analyzed layer, indicating that conventional models of ferromagnetism in random alloys are not appropriate; it has been suggested[1] that if dopant rich regions are above the magnetic percolation threshold and are connected macroscopically, the T_C can be significantly enhanced compared to the homogeneous alloy. Our study provides new three-dimensional structural information that is needed to advance quantitative structure−property relationships in DMS materials, particularly new models of magnetism that take into account a nonrandom distribution of dopant atoms.

EXPERIMENTAL METHODS

The growth, structural, and composition characterization, and magnetic characterization of these Co and Mn codoped Ge films have been reported previously.[6,18,19] The sample chosen for this study is a superlattice consisting of twenty bilayers of doped and undoped Ge layers. The sample was grown by molecular beam epitaxy (MBE) on a Ge (001) substrate at a temperature of 250 °C and a growth rate of 0.01 nm/s, employing sequential doping of Co and Mn for each atomic layer of Ge. The deposition times for the doped (undoped) layers were 1200 s (230 s), yielding a thickness of 12.0 nm (2.3 nm). Layer thickness was controlled in situ by monitoring reflection high-energy electron diffraction (RHEED) oscillations,[6] and was measured ex-situ using X-ray fluorescence (XRF) spectroscopy and X-ray diffraction (XRD).[6,19] A nominal concentration of $Co_{0.073}Mn_{0.035}Ge_{0.892}$ ($Ge_{1.00}$) was estimated using in situ atomic absorption spectroscopy and ex-situ XRF spectroscopy.[6,19] The sample is a hole-mediated ferromagnetic semiconductor similar to other reported examples of thick epitaxial films of doped Ge,[3−9] and exhibits large anomalous Hall coefficients and strong positive magnetoresistance (>10 at 5 T).[6,18] It exhibits superparamagnetism at high temperatures and undergoes a ferromagnetic transition near 100 K instead of a superparamagnetic blocking transition, also similar to earlier reports.[6−9] Sample preparation for the local electrode atom probe (LEAP) analysis was carried out using focused ion beam (FIB) lift out and annular milling.[20,21] Pulsed-laser APT analysis was conducted using a LEAP 3000× (532 nm laser, 0.6 nJ pulses, 100 kHz pulse frequency) at an evaporation rate of 0.2% and a temperature of 80 K.

RESULTS AND DISCUSSION

The APT reconstruction accurately reproduces the stoichiometry and superlattice structure of the sample (Figure 1) as determined by independent measurements.[6,19] Clearly visible in the mass spectrum are the single isotopes of Co and Mn, the five isotopes of Ge, and H atoms from the ultrahigh vacuum background (Figure 1a).[22] No peaks were identified at higher mass-to-charge state ratios. The background counts, less than 4% of the total, are due to evaporation events uncorrelated with the laser pulsing. The full three-dimensional reconstruction (Figure 1b) shows the expected composition: alternating layers of undoped Ge and Ge codoped with Co and Mn. The layers shown here represents three full bilayers that are closest to the surface (i.e., farthest from the Ge substrate).

One-dimensional composition profiles along the growth direction reveal enhancements in the Mn and Co concentrations at the interfaces of the codoped Ge layers (Figure 1c). The Mn distribution shows approximately symmetric enhancement at each interface, which suggests that some Mn diffusion takes place during growth. The slight enhancement of the Co counterpart at the bottom interface and the shift between the two profiles are likely the result of the sequential doping process, where Co was the first in the evaporation sequence. The growth conditions were in fact chosen to enable Mn diffusion to and activation in substitutional sites, with high concentrations of substitutional Mn stabilized by codoping with Co. The similarities of the Co and Mn distributions suggest that they diffuse together, though the nonzero concentration of Co in the undoped layers (Figure 1c) may indicate that Co diffuses more, particularly at the bottom of the doped layer. The Co and Mn distributions also establish the interfacial width between the doped and undoped layers of ∼3 nm, which is consistent with the length scale of dopant decomposition discussed further below. This interfacial width is larger than the nominal measurement resolution, which is 0.3−0.5 nm laterally and as high as 0.1 nm along the analysis direction (the same as the growth direction).[23] We note, however, that surface diffusion of dopant species during APT analysis cannot be strictly excluded, and trajectory overlap could also influence the reconstructed interface width.

dx.doi.org/10.1021/jp208553g |J. Phys. Chem. C 2012, 116, 276–280

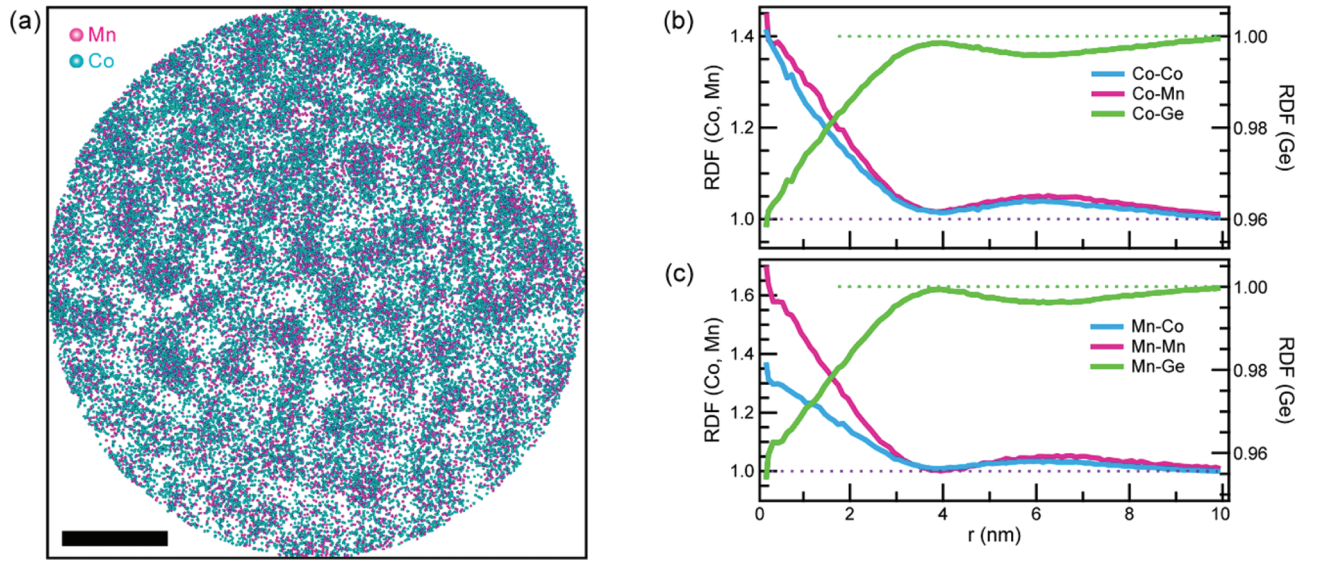

Figure 2. (a) Plan view of an individual codoped layer with 100% Co and Mn atoms displayed. Scale bar =10 nm. (b),(c) Radial distribution functions for Co (b) and Mn (c). The distributions of Ge about Co and Mn atoms are plotted on expanded axes to provide a more direct comparison of Ge matrix deficiencies with dilute Co and Mn enrichments.

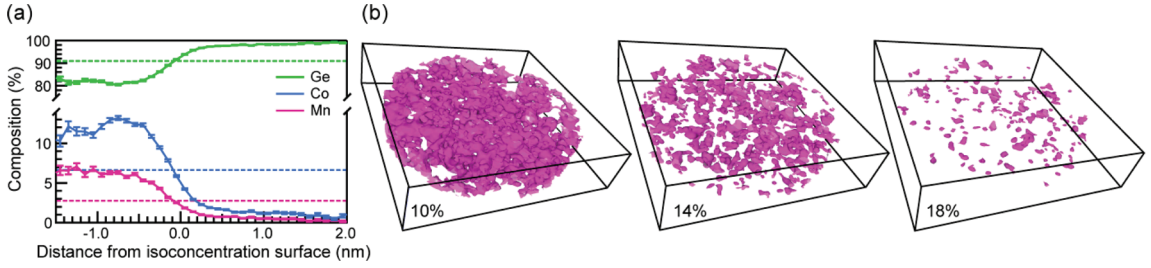

Figure 3. (a) Proxigram showing concentration as a function of distance from a 91% Ge isoconcentration surface, with average concentrations indicated by dotted lines. (b) Isoconcentration surfaces with increasing Co+Mn concentration (dimensions: 43 × 43 × 12 nm^3).

In addition to concentration enhancements along the growth direction, other projections and thin sections of the reconstruction demonstrate lateral and vertical inhomogeneity throughout the doped layers. In particular, regions enriched in Co and Mn atoms are visible upon inspection of a single codoped layer viewed from above (Figure 2a). The slightly greater apparent density of Co and Mn atoms at the top of Figure 2a is a reconstruction artifact arising from the deviation of the tip shape from a perfect hemisphere; the Ge density is equally affected, and therefore does not influence the analysis of variations in composition. Analysis using radial distribution functions (RDF, Figure 2b,c) demonstrates a positive correlation between the dopants, indicating the attractive interactions between Mn−Co, as well as Co−Co and Mn−Mn atoms. The IVAS v3.2 software package was used to calculate the RDFs with 0.1 Å thick shells, which were then smoothed with a weighted moving average binomial function as described by Sudbrack et al.[24] The RDFs demonstrate unequivocally the tendency for the two dopants to be found near each other, thus revealing an attraction between them. The Mn−Mn interaction exhibits the strongest correlation, suggesting that Mn atoms are most likely to be positioned near other Mn atoms. In addition the RDF analysis establishes the characteristic size (∼3 nm) and separation (∼6 nm) of the Co and Mn enriched regions.

Because magnetic interactions in regions with different dopant concentrations could differ, it is important to quantify the concentration of Mn and Co in dopant enriched regions and examine their morphology, specifically the shape and connectedness of the regions and their size. The fraction of Mn and Co contained within enriched regions was determined by generating a proximity histogram, or proxigram (Figure 3a) about an isoconcentration surface of the average Ge concentration (91%) in a single codoped superlattice layer. The average Mn (Co) concentration *inside* the isoconcentration surface (negative distance in Figure 3a) is 6% (12%), while the Mn (Co) concentration outside the enriched regions (positive distance in Figure 3a) is depleted to 1% (2%). Therefore, the majority of magnetically active species are found in the enriched regions. Further, it is possible to visualize the morphology and location of these regions by examining the Co+Mn isoconcentration surfaces at various concentrations (Figure 3b). The dopant enriched regions are dispersed throughout the layer and exist as both compact isolated volumes and as connected meandering volumes that span the entire layer depending on the choice of isoconcentration. At or below 10% Co+Mn concentration there are connected enriched regions that span the entire sample (Figure 3b), and 12% was the highest concentration that defined a single connected volume spanning the entire layer width. Enriched

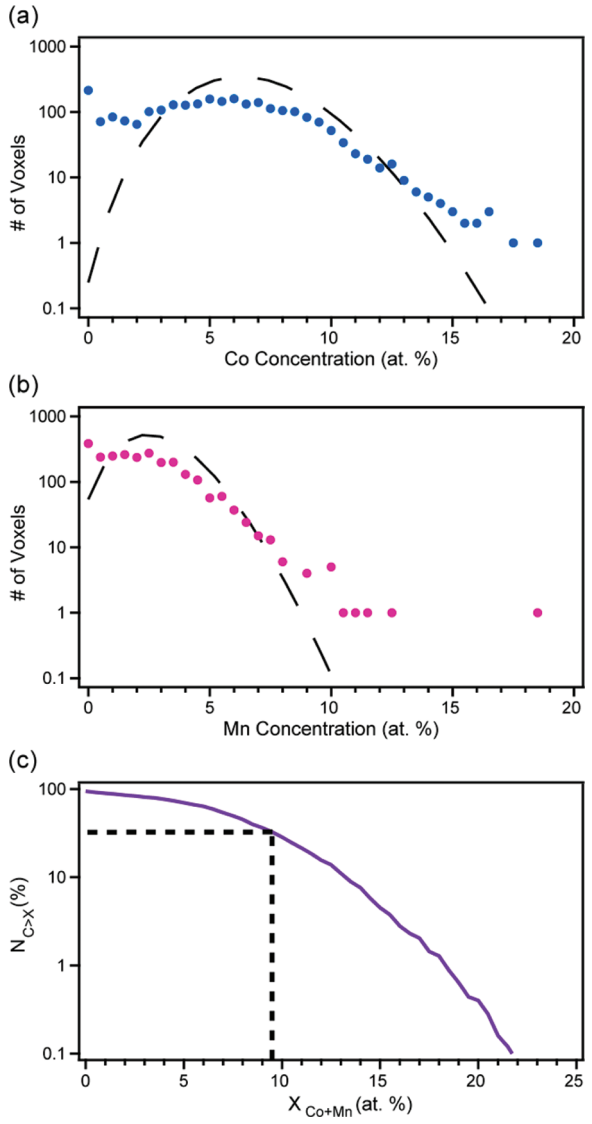

Figure 4. (a),(b) Frequency distribution of Co (a) and Mn (b) concentrations in 2 × 2 × 2 nm^3 voxels analyzed in 0.5 at % bins. The dashed lines correspond to a binomial distribution of voxels of a given dopant concentration as expected for a random alloy. (c) Percent of voxels N with a concentration of Co+Mn greater than x_{Co+Mn}. The vertical dotted line indicates the average concentration.

regions span the layer vertically but not laterally at 14%, and at concentrations of 18% and above the enriched volumes are isolated (Figure 3b).

The degree to which the distribution of Mn and Co atoms deviate from a random alloy on the nanometer length-scale was analyzed by comparing the frequency distribution of measured concentrations in finite 2 × 2 × 2 nm^3 "voxels" with a binomial distribution centered at the mean concentration (Figure 4). The voxel size, chosen to balance the dopant counting error against the resolution, resulted in ~200 detected atoms per voxel. Frequency distribution analysis was chosen over more sophisticated cluster identification algorithms because it can be applied efficiently to large data sets to provide quantitative determination of solute decomposition.[25,26] The frequency distributions of Co, Mn, and the random alloy were normalized to the total number of voxels. As shown in Figure 4, statistically significant deviations of the frequency distribution of Mn, Co, and Ge atoms from the binomial distribution (dashed lines of Figure 4a,b) are obvious. Specifically, deviations from the binomial distribution were found at Mn (Co) concentrations approximately below half and above twice the average values of 3% (6%). The volume fraction of the enriched regions was obtained from the frequency distribution, as shown in Figure 4c, enabling determination of the volume associated with a particular level of enrichment. For example, 33% of voxels have a concentration greater than the average concentration of 9.5% Co + Mn (dotted lines in Figure 4c). It is worth noting that less than 0.1% of voxels have dopant concentration greater than 22%; this concentration is less than 2 dopants per unit cell of the matrix, consistent with the presence of dimerized dopants.

CONCLUSIONS

Dopant decomposition in the absence of secondary phase formation was observed through APT analysis of a Co and Mn doped Ge thin film. The spatial variations in composition, particularly the connectedness of regions enriched in dopants, raise important questions about the origins of magnetism in DMS materials determined to be single phase by XRD and TEM. To date, much theoretical work has focused on percolation of magnetic interactions in random alloys, but this work indicates that many "real" materials might be better modeled as composite materials consisting of dopant rich and dopant poor regions. Macroscopic connections between the observed enriched regions, for example, may significantly enhance the Curie temperature compared to a random alloy. It is clear that APT can play a unique role in establishing a deeper understanding of magnetism in DMS materials.

AUTHOR INFORMATION

Corresponding Author

*E-mail: lauhon@northwestern.edu. Phone: 847-491-2232. Fax: 847-491-7820.

Present Addresses

[||]The Environmental and Molecular Science Laboratory, Pacific Northwest National Laboratory, Richland, WA 99352, U.S.A. E-mail: daniel.perea@pnnl.gov.

Author Contributions

J.R.R. and D.E.P. are cofirst authors.

ACKNOWLEDGMENT

We acknowledge the Office of Naval Research (N00014-09-0182), the National Science Foundation (DMR-0994433, DMR-1006069), and the Department of Energy (BES DE-FG02-05ER46216) for support of this work. J.R.R. was initially supported by the NSF REU program administered by the Northwestern University NSEC under EEC-0118025. Atom-probe tomographic measurements were performed in the Northwestern University Center for Atom-Probe Tomography (NUCAPT). The LEAP tomograph was purchased and upgraded with funding from NSF-MRI (DMR-0420532) and ONR-DURIP (N00014-0400798, N00014-0610539, N00014-0910781) grants. We also gratefully acknowledge the Initiative for Sustainability and Energy at Northwestern (ISEN) for grants to upgrade the capabilities of NUCAPT. We thank

Praneet Adusumilli for assistance with the sample fabrication and APT analysis.

REFERENCES

(1) Katayama-Yoshida, H.; Sato, K.; Fukushima, T.; Toyoda, M.; Kizaki, H.; Dinh, V. A.; Dederichs, P. H. *Phys. Status Solidi A* **2007**, *204*, 15–32.
(2) Pearton, S. J.; Park, Y. D.; Abernathy, C. R.; Overberg, M. E.; Thaler, G. T.; Kim, J.; Ren, F. *J. Electron. Mater.* **2003**, *32*, 288–297.
(3) Park, Y. D.; Hanbicki, A. T.; Erwin, S. C.; Hellberg, C. S.; Sullivan, J. M.; Mattson, J. E.; Ambrose, T. F.; Wilson, A.; Spanos, G.; Jonker, B. T. *Science* **2002**, *295*, 651–654.
(4) Dietl, T. *Nat. Mater.* **2010**, *9*, 965–973.
(5) Cho, S.; Choi, S.; Hong, S. C.; Kim, Y.; Ketterson, J. B.; Kim, B.; Kim, Y. C.; Jung, J. *Phys. Rev. B.* **2002**, *66*, 033303.
(6) Tsui, F.; He, L.; Ma, L.; Tkachuk, A.; Chu, Y. S.; Nakajima, K.; Chikyow, T. *Phys. Rev. Lett.* **2003**, *91*, 177203.
(7) Li, A. P.; Wendelken, J. F.; Shen, J.; Feldman, L. C.; Thompson, J. R.; Weitering, H. H. *Phys. Rev. B* **2005**, *72*, 195205.
(8) Kang, J. S.; Kim, G.; Wi, S. C.; Lee, S. S.; Choi, S.; Cho, S.; Han, S. W.; Kim, K. H.; Song, H. J.; Shin, H. J.; Sekiyama, A.; Kasai, S.; Suga, S.; Min, B. I. *Phys. Rev. Lett.* **2005**, *94*, 147202.
(9) Bougeard, D.; Ahlers, S.; Trampert, A.; Sircar, N.; Abstreiter, G. *Phys. Rev. Lett.* **2006**, *97*, 237202.
(10) Kuroda, S.; Nishizawa, N.; Takita, K.; Mitome, M.; Bando, Y.; Osuch, K.; Dietl, T. *Nat. Mater.* **2007**, *6*, 440–446.
(11) Bougeard, D.; Sircar, N.; Ahlers, S.; Lang, V.; Abstreiter, G.; Trampert, A.; LeBeau, J. M.; Stemmer, S.; Saxey, D. W.; Cerezo, A. *Nano Lett.* **2009**, *9*, 3743–3748.
(12) Ottaviano, L.; Passacantando, M.; Verna, A.; Gunnella, R.; Principi, E.; Di Ciccom, A.; Impellizzeri, G.; Priolo, F. *J. Appl. Phys.* **2006**, *100*, 063528.
(13) Zheng, R. K.; Moody, M. P.; Gault, B.; Liu, Z. W.; Liu, H.; Ringer, S. P. *J. Magn. Mater.* **2009**, *321*, 935–943.
(14) Coey, J. M. D. *Curr. Opin. Solid State Mater. Sci.* **2006**, *10*, 83–92.
(15) Lauhon, L. J.; Adusumilli, P.; Ronsheim, P.; Flaitz, P. L.; Lawrence, D. *MRS Bull.* **2009**, *34*, 738–743.
(16) Larson, D. J. *Thin Solid Films* **2006**, *505*, 16–21.
(17) Kodzuka, M.; Ohkubo, T.; Hono, K.; Matsukura, F.; Ohno, H. *Ultramicroscopy* **2009**, *109*, 644–648.
(18) Collins, B. A.; Chu, Y. S.; He, L.; Zhong, Y.; Tsui, F. *Phys. Rev. B.* **2008**, *77*, 193301.
(19) Tsui, F.; Collins, B. A.; He, L.; Mellnik, A.; Zhong, Y.; Vogt, S.; Chu, Y. S. *Appl. Surf. Sci.* **2007**, *254*, 709–713.
(20) Thompson, K.; Lawrence, D.; Larson, D. J.; Olson, J. D.; Kelly, T. F.; Gorman, B. *Ultramicroscopy* **2007**, *107*, 131–139.
(21) Miller, M. K.; Russell, K. F.; Thompson, K.; Alvis, R.; Larson, D. J. *Microsc. Microanal.* **2007**, *13*, 428–436.
(22) Perea, D. E.; Wijaya, E.; Lensch-Falk, J. L.; Hemesath, E. R.; Lauhon, L. J. *J. Solid State Chem.* **2008**, *181*, 1642–1649.
(23) Seidman, D. N. *Annu. Rev. Mater. Res.* **2007**, *37*, 127–158.
(24) Sudbrack, C. K.; Noebe, R. D.; Seidman, D. N. *Phys. Rev. B.* **2006**, *73*, 212101.
(25) Moody, M. P.; Stephenson, L. T.; Ceguerra, A. V.; Ringer, S. P. *Microsc. Res. Tech.* **2008**, *71*, 542–550.
(26) Stephenson, L. T.; Moody, M. P.; Liddicoat, P. V.; Ringer, S. P. *Microsc. Microanal.* **2007**, *13*, 448–463.